ELSEVIER

Journal of Power Sources 81–82 (1999) 335–339

JOURNAL OF POWER SOURCES

www.elsevier.com/locate/jpowsour

Structure and electrochemical properties of anodes consisting of modified SnO

Hong Li, Xuejie Huang, Liquan Chen *

Laboratory for Solid State Ionics, Institute of Physics, Chinese Academy of Sciences, Beijing 100080, China

Abstract

A series of composite SnO materials were prepared by mixing SnO powder with reducing agents and heating at different temperatures for different periods under argon atmosphere. It was found that α-SnO with its tetragonal structure could transform into the β-Sn phase or orthorhombic SnO depending on treatment conditions. The electrochemical behaviors of these materials used as an anode active material in lithium rechargeable batteries was investigated. It was found that excessive amounts of reducing agents, especially in the case of carbon black, may provide a good dispersion environment for SnO which is similar to the case of amorphous tin composite oxides (TCO). The presence of β-Sn or orthorhombic SnO is not beneficial to the cycling performance, although a large ratio of β-Sn in the starting anode material can decrease the capacity loss during the first cycle. Superfine SnO material was also prepared by decomposing SnC_2O_4 which was synthesized by a sol–gel method. Its cyclic performance was improved significantly.

Keywords: SnO anode; XRD; Lithium ion batteries; Electrochemical properties

1. Introduction

Since Fuji Photo Film has filed a patent using amorphous tin composite oxides (TCO) as active anode materials for rechargeable lithium batteries [1], metal oxide anodes have attracted much attention due to their large reversible capacity [2].

Tin oxide anodes have different discharge and charge mechanism compared to carbonaceous anodes. Courtney and Dahn [3], Liu et al. [4] and Li et al. [5] have reported a two-step reaction mechanism for the reaction of lithium with SnO_2 and SnO based on their analyses of in-situ XRD, Raman data and HRTEM. In the first step, SnO_x is replaced by lithium to produce irreversibly amorphous Li_2O and Sn. In the second step, tin combines with lithium to form various Li–Sn alloys. Furthermore, according to our results from HRTEM [5], FTIR [6] and impedance spectra [7], another source of irreversible capacity loss is confirmed to be related to the electrolyte decomposition reaction on the surface of the SnO anode, which is similar to the case of carbon or metallic lithium anodes [6,8–10]. This scenario explains the reversible capacity of SnO anode in terms of an alloying process instead of intercalation, while the irreversible capacity is predominantly caused by the replacement reaction of SnO and the electrolyte decomposition reaction. The main electrochemical reactions of the metal oxide anode are listed as follows:

$$(2y - x)\mathrm{Li}^- + \mathrm{Li}_x\mathrm{MO}_y + (2y - x)\mathrm{e}^- \rightarrow y\mathrm{Li}_2\mathrm{O} + \mathrm{M} \quad (x \geq 0) \tag{1}$$

$$x\mathrm{Li} + \mathrm{M} + x\mathrm{e}^- \leftrightarrow \mathrm{Li}_x\mathrm{M} \tag{2}$$

$$\mathrm{Li}^- + \text{electrolyte}\,(\mathrm{EC}, \mathrm{DEC}, \mathrm{LiPF_6}, \ldots) + \mathrm{e}^- \rightarrow \mathrm{SEI}\,(\mathrm{Li_2CO_3}, \mathrm{ROCO_2Li}, \ldots) \tag{3}$$

It is well known that lithium alloys have been investigated as anodes in rechargeable lithium batteries since 1970s [11]. The main problem of Li-alloy anode materials is the significant differences in volume between the Li-alloys and the pure basis metals [12]. Various attempts have been undertaken to enhance the dimensional stability of Li-alloy electrodes [13,14]. Recently, Besenhard et al. [15] confirmed that dimensional changes and pulverization fail-

* Corresponding author. Fax: +86-10-62562605; E-mail: lqchen@aphy02.iphy.ac.cn

0378-7753/99/$ - see front matter
PII: S0378-7753(99)00212-8

ure of Li-alloy electrodes during cycling can be minimized in small particle size multiphase alloy matrices. It was also found that an anode consisting of nanometer size SnO prepared by ball milling showed better cycling performance than a normal SnO anode [16]. Courtney and Dahn [17] also suggested that TCO materials with small particles and small grains give the best performance. Therefore, it can be concluded that the microstructure for either metal oxide anodes or alloy anodes has an important influence on the cycling performance.

Furthermore, according to Eq. (1), it is easy to understand that the irreversible capacity loss is related to the oxygen content of the original metal oxides. Compared to SnO, for example, SnO_2 consumes two more moles of Li ions per Sn atom according to the replacement reaction (1). Thus, controlling the oxidation state of M may also be important to decrease the irreversible capacity loss.

In this work, a series of composite materials based on pure SnO were prepared. Their structure and electrochemical properties were compared.

Table 1
Discharge and charge properties of treated SnO at different conditions

Sample number	Treatment condition (weight ratio)	Phase[a]	Dis. 1 (mA h/g)	Efficiency (%)	Dis. 10[b] (mA h/g)	Efficiency (%)	Total efficiency (%)
SN02	Pure A.R. SnO	α-SnO	890	88.3	500	95.8	56.1
SN03	Pure A.R. SnO_2		1200	58.3	400	95.2	33.3
SN04	SnO/CuO/CB (2:1:0.01), 900°C, 4 h	β-Sn (H.P. SnO)	440	78.4	220(6)	97.8	50
SN05	SnO/CB (3:1), 900°C, 4 h	β-Sn	420	78.4	350(5)	94.1	83.3
SN08	SnO/CB (50:1), 900°C, 4 h	β-Sn (α-SnO)	800	80.0	150(4)	93.3	18.8
SN09	SnO/CB (30:1), 900°C, 4 h	β-Sn (α-SnO)	685	41.0	112(5)	74.1	16.3
SN10	SnO/CB (120:1), 400°C, 5 h	α-SnO	1020	69.1	480	92.0	47.1
SN11	SnO/CB (60:1), 400°C, 5 h	α-SnO	1181	73.6	560	97.9	47.4
SN12	SnO/CB (120:1), 500°C, 5 h	α-SnO	880	56.8	150(8)	83.3	17.0
SN13	SnO/CB (60:1), 500°C, 5 h	H.P. SnO + α-SnO	920	54.3	140(7)	90.9	15.2
SN14	SnO/CB (60:1), 400°C, 9 h	α-SnO	1104	72.7	459	97.3	41.6
SN15	SnO/CB (60:1), 400°C, 2 h	α-SnO	1049	59.8	665	98	63.3
SN16	SnO/CB (10:1), 400°C, 2 h	α-SnO	975	71.8	600	98.0	61.5
SN17	SnO/CB (10:1), 400°C, 5 h	α-SnO	1004	65.7	575	98.0	57.3
SN18	SnO/CB (6:1), 400°C, 5 h	α-SnO	1100	69.0	600	98.0	54.5
SN19	SnO, 400°C, 7 h	α-SnO	720	73.4	450	95	62.5
SN20	SnO/CB (10:1), 400°C, 7 h	α-SnO + H.P. SnO	1054	70.7	686	99.0	65.1
SN21	SnO/CB (10:1), 500°C, 5 h	H.P. SnO (β-Sn)	760	84.2	330(7)	78.5	43.4
SN22	SnO/CB (6:1), 500°C, 5 h	H.P. SnO + β-Sn	789	96.4	507	96.2	64.3
SN23	SnO/GP/Fe (10:1:2), 500°C, 5 h	H.P. SnO + β-Sn	842	73.2	429(8)	95	50.9
SN24	SnO/CB (10:1), 400°C, 9 h	α-SnO (H.P. SnO)	1100	65.4	450	93.1	40.9
SN25	SnO/GP (10:1), 400°C, 9 h	α-SnO (H.P. SnO)	973	59.1	330(8)	90	33.9
SN37	♠, 400°C, 6 h	α-SnO	1320	72.7	720	98.5	54.5
TCO*	$SnSi_xP_yO_{2+z}$, 1100°C		1030	63.0	550		53.4

Efficiency = $Cap._{charge}/Cap._{discharge}$. Total efficiency = $Cap._{dis.\ 10}/Cap._{dis.\ 1}$.
· Data from Ref. [2].
[a]The phase in brackets means that correspondent peaks are weak in XRD pattern.
[b]The number in brackets means real cycle number.

2. Experimental

2.1. Sample preparation and characterization

Most of the samples were prepared by mixing SnO powder with a reducing agent, such as carbon black, Cu_2O, Fe or graphite powder. Then, the mixtures were pressed into pellets and heated at various temperatures from 350 to 900°C in argon atmosphere. The preparation conditions for various samples are listed in Table 1. The pellets were subsequently ground and passed through a 325-mesh screen.

SN37 was prepared by a sol–gel method. Firstly, $SnCl_2 \cdot H_2O$ salt was dissolved in alcohol to form a 0.5-M $SnCl_2$ solution. Then, 0.5 M of an aqueous solution of $H_2C_2O_4$ was slowly dropped into the alcohol solution of $SnCl_2$ while the mixture was constantly stirred. After $H_2C_2O_4$ had been added in a slight excess, diluted ammonia was gradually dropped into the mixture until a light yellow milky gel formed at pH = 7. Finally, after filtering and drying, the resulting white sol was heated at 400°C for 5 h under argon.

The crystal structure of the samples was analyzed using a Rigaku B/max-2400 X-ray diffractometer equipped with Fe Kα radiation.

2.2. Electrochemical testing

Electrodes were prepared by coating a copper foil substrate with the slurry of the active material (87 wt.%), carbon black (8.7 wt.%) and polyvinylidene fluoride (PVDF) (4.3 wt.%) dissolved in cyclopentanone. After coating, the slurry was dried at 120°C for 8 h under vacuum and then pressed between two stainless steel plates at 1 MPa. Prior to cell assembling, the electrodes whose area was 0.6 cm^2 were dried at 120°C for 4 h under vacuum. The test cells had a typical two-electrode construction using polypropylene microporous sheet as the separator, 1 M $LiPF_6$ dissolved in ethyl carbonate (EC) and diethyl carbonate (DEC) (1:1 v/o) as the electrolyte, a pure lithium foil as the negative electrode and the metal oxide film described above as the working electrode. The cells were assembled in an argon-filled glove box. The cells were charged and discharged at a constant current of 0.20 mA/cm^2 and cycled between 0.00 and 2.000 V.

3. Results and discussion

3.1. Structure characterization of modified SnO materials

The tetragonal α-SnO used as a raw material in this work could be transformed into other phases depending on the preparation conditions. According to Table 1, it was found that α-SnO could be reduced to β-Sn phase or transformed into the orthorhombic phase SnO (named orth-SnO) [18]. Fig. 1 shows the XRD patterns of three typical samples, SN08, SN21 and SN24 where the phases were identified using the data from JCPDS [18]: SN08 was mainly composed of β-Sn, SN21 was mainly composed of orth-SnO, also included a little of β-Sn, while SN24 is composed of α-SnO and a little of orth-SnO.

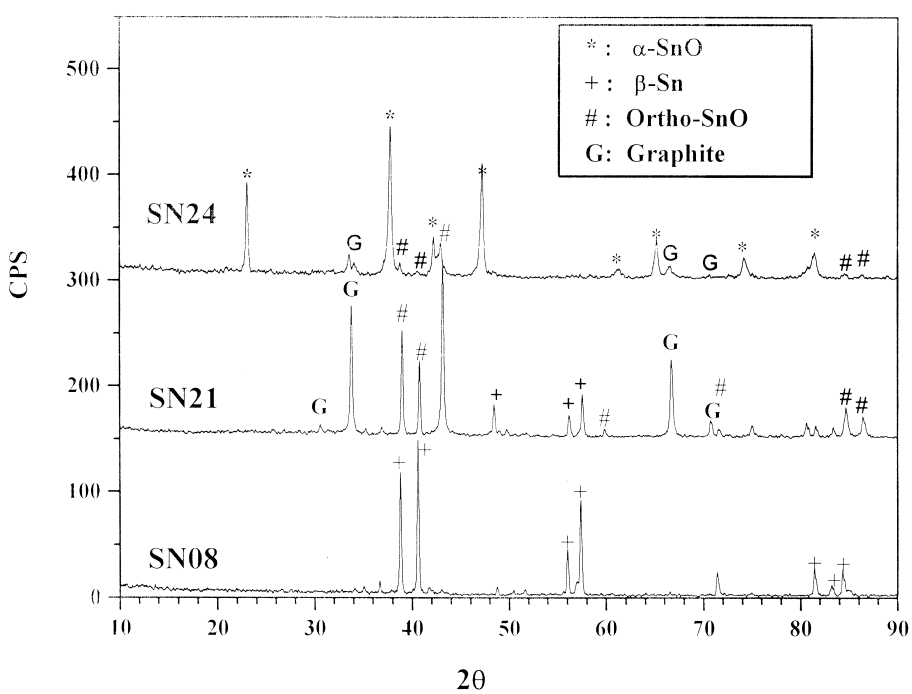

Fig. 1. XRD patterns of treated composite SnO samples (Fe target, 1.9373λ) SN08:SnO/CB (50:1), 900°C, 4 h, SN21:SnO/CB (10:1), 500°C, 5 h, SN24:SnO/CB (10:1), 400°C, 9 h.

3.2. Electrochemical properties of modified SnO materials

The electrochemical properties of the samples depend on the electrode phases which was demonstrated in the galvanostatic cycling curves shown in Fig. 2. Combined with the data in Table 1, the discussion on the relation between the phase composition and the electrochemical properties of these samples is divided into four sections.

3.2.1. The presence of β-Sn

Above 500°C, SnO could be reduced by carbon black or graphite. Once metallic Sn was produced, these dispersed fine grains of Sn had a strong affinity to form many Sn beads, especially when heated at 900°C which is much higher than the melting point of metallic Sn (232°C). Samples with larger Sn beads originated finally from the powder passed through a 325-mesh screen. It was found that the cycling performance of SN05 was better than SN08 and SN09 (see Table 1 and Fig. 2). The difference between these three samples is the amount of carbon black used in the reduction process of the SnO powder. Since complete reduction of SnO only need carbon black less than 10% of its weight based on Eq. (4):

$$SnO + C \rightarrow Sn + CO \quad (4)$$

Excess carbon black in SN05 may act as a dispersion medium, thus improve the cycling performance. Based on reaction (2), if lithium can alloy Sn to $Li_{4.4}Sn$, the total capacity will be 992 mAh/g Sn. Furthermore, if the active material is pure metal, the irreversible capacity loss caused by replacement reaction (1) can be eliminated. The efficiency of SN22 was found higher than most of the other samples. However, the presence of Sn with a larger particle size is not beneficial to the cycling performance [15]. We have also investigated the microstructure of SnO at a deep discharge state using HRTEM [5]. It was found that the Li–Sn alloy phases consisted of many small crystallites (< 3 nm) along with a few larger crystallites (< 20 nm) were highly interspersed with an amorphous Li_2O matrix underneath a surface film [5]. This may be the reason why metal oxide anodes have a better cycling performance than alloy anodes. However, it is difficult to disperse nanosize Sn grains into a medium by annealing because these grains tend to agglomerate to beads at elevated temperature.

3.2.2. The electrochemical behavior of orth-SnO

Sample SN21 mainly consisted of orth-SnO and was heated at 500°C for 5 h in argon. The cycling performance is much worse than SN17 (see Fig. 2 and Table 1). This also holds true when comparing SN24 with SN16, SN17. Although the presence of orth-SnO was also detrimental to the cycling performance, its influence was less serious than β-Sn. In addition, the reaction processes of orth-SnO had to be similar to α-SnO judged from the shape of the discharge curves of SN21, SN22 and SN37.

3.2.3. The function of carbon black or graphite

According to the heat treatments, the samples can be divided into different groups: (a) 900°C, 4 h, SN05, SN08,

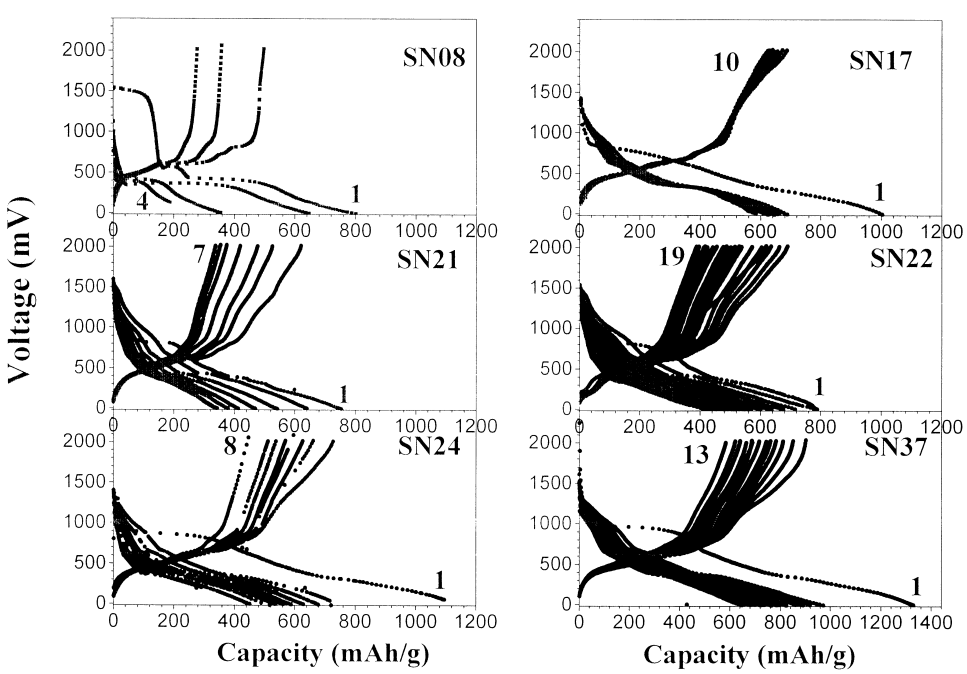

Fig. 2. The discharge and charge curves of treated composite SnO samples. SN08:SnO/CB (50:1), 900°C, 4 h, SN17:SnO/CB (10:1), 400°C, 5 h, SN21:SnO/CB (10:1), 500°C, 5 h, SN22:SnO/CB (6:1), 500°C, 5 h, SN24:SnO/CB (10:1), 500°C, 9 h, SN37:SnO prepared by sol–gel.

SN09; (b) 400°C, 5 h, SN10, SN17, SN18; (c) 500°C, 5 h, SN12, SN21, SN22; and (d) 400°C, 9 h, SN14, SN24, SN25.

From Table 1, it is easy to see that in each group the samples prepared with more carbon black showed a better cycling performance. As mentioned before, only 10 wt.% carbon black was necessary for the reduction of SnO. At 400°C, carbon black barely reduced SnO based on data from Table 1. In this case, carbon black only observed as a good conductivity additive. In general, the conductivity of all of the samples was already high since all electrodes were prepared by mixing 8.7 wt.% carbon black with the active materials. Therefore, excessive carbon black in the electrodes could not increase the conductivity significantly. Carbon black is composed of many nanometer size graphene crystallites. It has strong deformability. Courtney and Dahn have supposed that amorphous TCO have better cycling performance related to their small grains and a stable Li_2O matrix [13,15]. Excess carbon black may play a similar role as a dispersion medium. It is believed that a stable and plastic dispersion medium can endure a larger volume variation during cycles thus improving the cycling performance of alloy processes. This may be confirmed by comparing the electrochemical behavior of SN24 and SN25, where, according to Table 1, SN24 which was mixed with plastic carbon black showed a better cycling performance than sample SN25 which was mixed with the harder graphite.

3.2.4. The electrochemical behavior of SnO prepared by the sol–gel method

Based on the discussion above, samples consisting of small particles which were dispersed in a plastic and stable medium had a better cycling performance. Therefore, we prepared SnO by decomposing SnC_2O_4 which was synthesized by the sol–gel method. It is a widely used method to obtain superfine particles [19–21]. The resulting SnO powder was brown and wadding. The cycling performance of SN37 was much better than all the other samples (see Fig. 2 and Table 1). By delivering a reversible capacity of 720 mAh/g at the tenth cycle at 100% DOD (cycled between 0.0 to 2.0 V), however, the irreversible capacity loss after 20 cycles exceeded 50% of the initial capacity.

4. Conclusions

A series of composite SnO materials were prepared by mixing SnO powder with reducing agents and heated at different temperatures for different periods under argon atmosphere. Above 500°C, tetragonal α-SnO was reduced to β-Sn phase. The presence of β-Sn with its larger crystallite size reduced the capacity loss during the first cycle, but also decreased the cycling performance significantly. It was found that α-SnO can also be transformed into orthorhombic SnO depending on the treatment conditions, but this is not beneficial to the cycling performance. It was confirmed that an excessive amount of reducing agents in the active materials, in particular carbon black, provided a good dispersion environment for SnO thereby improving the cycling performance, similar to the amorphous network in TCO. It was also found that SnO prepared by the sol–gel method showed a better capacity retention due to the formation of smaller grains.

Acknowledgements

This work was supported by Ford-NSFC Foundation (contact No. 9712304), NSFC (contact No. 59672027) and National 863 Key Program (contact No. 715-004-0280).

References

[1] Y. Idota, M. Nishima, Y. Miyaki, T. Kubota, T. Miyasaki, European Patent, 0651450A1, 1995.
[2] Y. Idota, T. Kubota, A. Matsufuji, Y. Maekawa, T. Miyasaka, Science 276 (1997) 1395.
[3] I.A. Courtney, J.R. Dahn, J. Electrochem. Soc. 144 (1997) 2045.
[4] W.F. Liu, X.J. Huang, Z.X. Wang, H. Li, L.Q. Chen, J. Electrochem. Soc. 145 (1998) 59.
[5] H. Li, X.J. Huang, L.Q. Chen, Electrochem. Solid State Lett. 1 (6) (1998) in press.
[6] H. Li, J.Z. Li, Z.X. Wang, X.J. Huang, L.Q. Chen, submitted.
[7] H. Li, X.J. Huang, L.Q. Chen, submitted.
[8] A.N. Dey, J. Electrochem. Soc. 118 (1971) 1547.
[9] R. Fong, U.V. Sacken, J.R. Dahn, J. Electrochem. Soc. 137 (1990) 2009.
[10] D. Aurbach, M.L. Daroux, P.W. Faguy, E. Yeager, J. Electrochem. Soc. 134 (1987) 1611.
[11] J. Yang, M. Winter, J.O. Besenhard, Solid State Ionics 90 (1996) 281.
[12] J.O. Besenhard, M. Hess, P. Komeda, Solid State Ionics 40/41 (1990) 525.
[13] R.A. Huggins, J. Power Sources 26 (1989) 109.
[14] B.A. Boukamp, G.C. Lesh, R.A. Huggins, J. Electrochem. Soc. 128 (1980) 725.
[15] J.O. Besenhard, J. Yang, M. Winter, J. Power Sources 68 (1997) 87.
[16] H. Li, X.J. Huang, L.Q. Chen, Solid State Ionics, in press.
[17] I.A. Courtney, J.R. Dahn, J. Electrochem. Soc. 145 (1998) 2943.
[18] α-SnO: JCPDS, No. 5-0390; β-Sn: JCPDS, No. 4-0673; orth-SnO: JCPDS, No. 24-1342.
[19] M.A. Butlar, P.F. James, J.D. Jacken, J. Mater. Sci. 31 (1996) 1675.
[20] P.A. Buining, L.M. Liz-Marzan, A.P. Philipse, J. Colloid Interface Sci. 179 (1996) 318.
[21] N. Ichinose, Y. Ozaki, S. Kashu, Superfine Particle Technology, Springer-Verlag, London, 1992.